Co-Fe-Ce co-doped TiO_2 nanoparticles for Photocatalytic Application under visible irradiation

Anju Rani[1], R. L. Dhiman[2], Virender Singh[3], Suresh Kumar[3] and Suresh Kumar[1,4]
[1]Department of Physics, M.M. University, Sadopur, Ambala - 134 007 India
[2]Department of Physics, Sanatan Dharma College, Ambala Cantt.- 133 001 India
[3] Department of Electronic Science, Kurukshetra University, Kurukshetra - 136 119 India
[4]Department of Physics, M.M. (Deemed to be University), Mullana-Ambala-133 207 India

[2]Email: roshandhiman_kuk@yahoo.co.in

Abstract

Cobalt, Iron & Cerium co-doped $Co_xFe_{0.02}Ce_{0.02}Ti_{0.96-x}O_2$; x = 0.02, 0.03 & 0.04 mol % nanoparticles were fabricated by following sol-gel process. Characterization of synthesized samples was carried out through X-ray diffraction, UV-visible and Fourier transform infrared spectroscopy, Transmission electron and Field-emission scanning electron microscopy and Electron dispersive X-ray spectroscopy. Anatase phase of fabricated nanoparticles was estimated by XRD and further verified by EDXS measurements. Using Debye Scherrer's formula the particle size of synthesized nanoparticles calculated was 24.8 to 10.3 nm. With growing cobalt concentration (x) shifting of absorption edge towards region of higher wave length correspond to blue shift as noticed from UV–Visible absorption spectra indicate the generation of energy sub states within forbidden gap and reduction in energy band gap from 2.57 eV to 1.69 eV. Structural formation of the synthesized nanoparticles was studied by FTIR spectroscopy which confirm that formed TiO_2 nanoparticles have stable anatase pahse. Photocatalytic degradation activity against congo red and methyl orange dyes was detected by visible light illumination. Observations showed that with rise in cobalt concentration (x) the photocatalytic activity rises which is ascribed to decreasing rate of carrier recombination and increasing surface area of the fabricated nanoparticles.

Keywords: Nanoparticles, Photocatalytic activity

1. Introduction

Photocatalysis is a chemical reaction steped up in presence of a catalyst and light photons [1]. In recent years Researchers have focused more attention on Photocatalysis process because it is inexhaustible, nonhazardous, clean, safe source of energy and economically viable, facile process towards organic transformation using light [2-3]. Photocatalysis based on semiconductor metal oxides as photocatalysts used for wastewater treatment and degradation of toxic and non biodegradable organic pollutants to harmless compounds [4-5]. Semiconductor metal oxides e.g TiO_2 is most suitable because of its tuneable band gap, band edge positions, low cost, non-toxicity, high chemical and thermal stability, non-toxicity, resistance to photochemical and chemical erosion etc. [6]. TiO_2 nanoparticles can exist in both anatase as well as in rutile phase. It has been accepted that the photocatalytic efficiency exhibited by anatase phase is higher compared to rutile one [7]. It was reported that doping of iron in TiO_2 can help in conversion of phase from amorphous to anatase as TiO_2 as amorphous is not photoactive because of having broad band

gap (3.2 eV) and quick electron-hole recombination [8-9]. Researchers have made significant contributions in tailoring the band gap on substitution of suitable dopent in TiO_2 nanoparticles synthesized by different techniques in order to enhance the photocatalytic activity. Chekuri et al. have synthesized TiO_2 nano materials doped with cobalt, assisted by gemini surfactant and observed enhance photocatalytic activity [10]. Synthesized cobalt doped TiO_2 nanoparticles leads to excellent photocatalytic degradation activity for methyl orange when irradiated with both UV as well as visible light [11]. Ganesh et al. prepared different amount of Fe doped TiO_2 nanoparticles fabricated by conventional co-precipitation technique and dried at temperature range 400 -800^{o}C. It was reported that the lower amount of iron doped TiO_2 nanoparticles gives higher response towards degradation of Methylene blue [12]. Xiao-Jun Li et al. reported that individual substitution of iron and cerium in TiO_2 iron gets introduced however cerium does not enter in the framework of TiO_2. On co-doping of iron and cerium, both were introduced in TiO_2 framework and provides much more intense surface hydroxyl concentration having high photocatalytic degradation as compared to the separately doped TiO_2 [13]. This work comprises the study of consequence of doping of cobalt on degradation efficiency against methyl orange and congo red dye. We have planned to synthesize $Co_xFe_{0.02}Ce_{0.02}Ti_{0.96-x}O_2$; x = 0.02, 0.03 & 0.04 mol % nanoparticles by following sol-gel process. Following techniques have been used to study structural, morphological and optical characteristics of the fabricated nanoparticle samples; X-ray Diffraction, Field emission scanning electron microscopy, Energy dispersive X-ray spectroscopy, Transmission Electron Microscopy, UV-Visible spectroscopy and Fourier transform infrared spectroscopy. Photocatalytic degradation activity against congo red and methyl orange dyes was detected under visible light illumination.

2. Experimental Details

2.1 Sample preparation

For the synthesis of present nanoparticles we have used all AR grade chemicals e.g. Titanium (IV) tetraisopropoxide ($C_{12}H_{28}O_4Ti$, 97%), Cobalt (II) Nitrate ($Co(NO_3)_2.6H_2O$, 99%), Cerium (III) Nitrate hexahydrate ($Ce(NO_3)_3.6H_2O$, 99%) and Ferric Chloride ($FeCl_3$, 98%). All compositions were prepared using DI water and methanol (CH_3OH, 99.8%). All glassware were washed properly with DI water and dried well before use. Different composition of TiO_2 nanoparticles co-doped with cobalt, iron and cerium were prepared by controlled sol-gel technique using an appropriate amount of pure metal salts as mentioned above. Details of synthesis process as follows; titanium (IV) isopropoxide (13 ml) in methanol (50 ml) was poured drop by drop under vigorous stirring into small amount of DI water containing 0.29 gm of Cobalt (II) Nitrate (adjusted to appropriate pH with 0.8 ml conc. HNO_3). Then after violent stirring of 1 hr a solution consisting of 0.16 gm of Cerium (III) Nitrate hexahydrate and 0.43 gm of Ferric chloride in DI water (small amount) was poured to it drop by drop with continuous stirring and mixture for 4 h was stirred at room temperature until it became a transparent greenish sol. Then the sol was kept overnight to form gel, which was then dried at 100^{o}C for 24 h in vacuum oven to eliminate the solvents from gel. After that it was grinded to powder by agate mortar. Finally the resulted powder was annealed at 400^{o}C in an electric furnace for 4 h to obtain crystalline powder of codoped TiO_2 nanoparticles. Other compositions were also prepared at same experimental conditions. Figure 1 is displaying graphical representation of fabrication process.

2.2 Characterization of synthesized nanoparticles

By making use of Cu-Kα radiation having wavelength, λ= 1.5406 Å at room temperature XRD patterns were recorded to verify single phase formation of fabricated nanoparticle samples. FTIR spectra were also recorded at room temperature to further confirm the stable phase formation of co-doped nanoparticles of TiO_2. By using Scanning Electron Microscope (Zeiss Evo 40 analytical), synthesized nanoparticles were studied for surface morphology. The presence of elements in all fabricated samples was detected using EDX spectrometer. To verify nanoparticle formation the TEM images using Hitachi (H-7500) microscope were recorded. Utilising UV-visible absorption spectroscopy, optical band gap of synthesized samples have been found. Photocatalytic degradation activity against congo red and methyl orange dyes was determined as follows: To attain an adsorption/desorption equilibrium, 100 ml dye solution (10^{-5} mol/liter) containing 0.05 gm of co-doped TiO_2 nanoparticles was stirred in dark for 1 hr. The suspension was then stirred by illuminating from the top for 120 minutes by phosphorus coated mercury vapour lamp having cut off filters consisting 420 nm to 520 nm wavelength. After regular intervals (20 min) of illumination, about 3 ml sample from the dye dissolved solution was taken out and then centrifuged on after filtration analyzed by UV-Vis spectrophotometer taking DI water as a reference. No degradation of dyes was observed in absence of light.

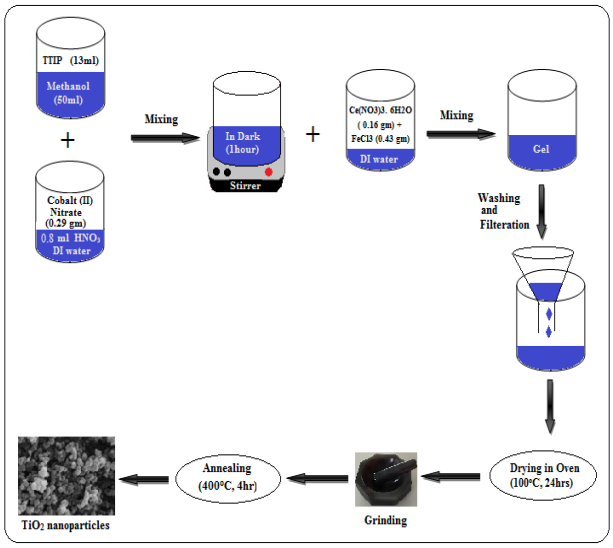

FIG 1. Pictorial representation of synthesis process.

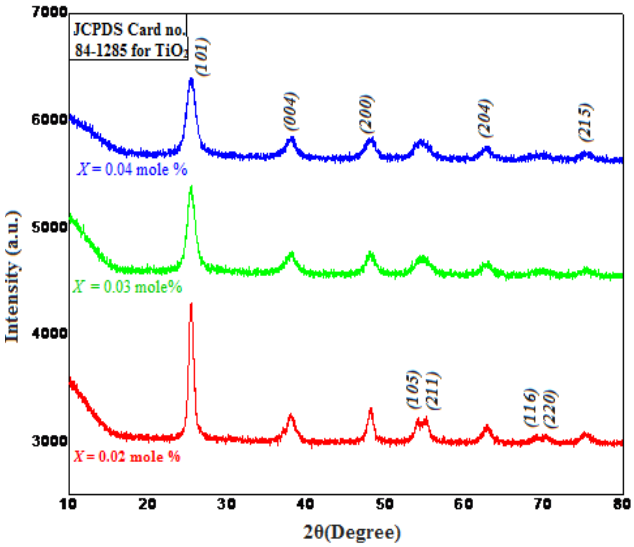

FIG 2. X-ray Diffraction pattern of fabricated nanoparticles.

3. Results and Discussion

3.1 Structural analysis

XRD pattern of fabricated $Co_xFe_{0.02}Ce_{0.02}Ti_{0.96-x}O_2$; x = 0.02, 0.03 & 0.04 mol % nanoparticle samples is displayed in Figure 2. In co-doped TiO_2 nanoparticles anatase phase formation was verified from diffraction peaks appeared at 2θ values 25.41°, 38.1°, 48.1°, 54.2°, 55.1°, 62.9°, 68.9°, 70.4° and 75.3° corresponding to the crystal planes (1 0 1), (0 0 4), (2 0 0), (1 0 5) (2 1 1) (2 0 4) (1 1 6) (2 2 0) and (2 1 5) respectively. All diffracted peaks are found to be in accordance with standard diffraction data of the anatase phase (JCPDS file no. 84-1285). Using FWHM of most dominated (101) peak of XRD the calculation of size of nanoparticles was browned by using Debye-Scherrer equation [14].

$$D = \frac{k\lambda}{\beta \cos\theta} \quad (1)$$

Here K = 0.89 (shape factor), λ represents wavelength of X-rays having value 0.154 nm, θ represents diffraction angle in radians, β is FWHM of (101) peak and D is size of nanoparticles in nm. Particle size of synthesized co-doped TiO_2 nanoparticles found to be 24.8 nm to 10.3 nm are listed in Table 1. The calculated particle size decreases slightly with increasing molar concentration of dopant. Moreover, the diffraction peaks got broaden after doping which indicates that the particle size of synthesized nanoparticles decreases on further doping.

3.2 Elemental analysis

The elemental presence in prepared samples was detected by EDXS. Figure 3(a-c) shows approximately 1:2 peak ratio of Ti and O as estimated from the O peak at 0.523 keV and the Ti peaks at 0.4 and 4.51 keV. The present analysis confirmed that the amount of cobalt, iron and cerium are in good agreement with the base compositions and positions of peaks for Co at 0.798 and 6.95 keV, Fe at 0.7 and 6.4 keV and Ce at 0.89 and 4.85 keV were found to be same for all synthesized nanoparticles

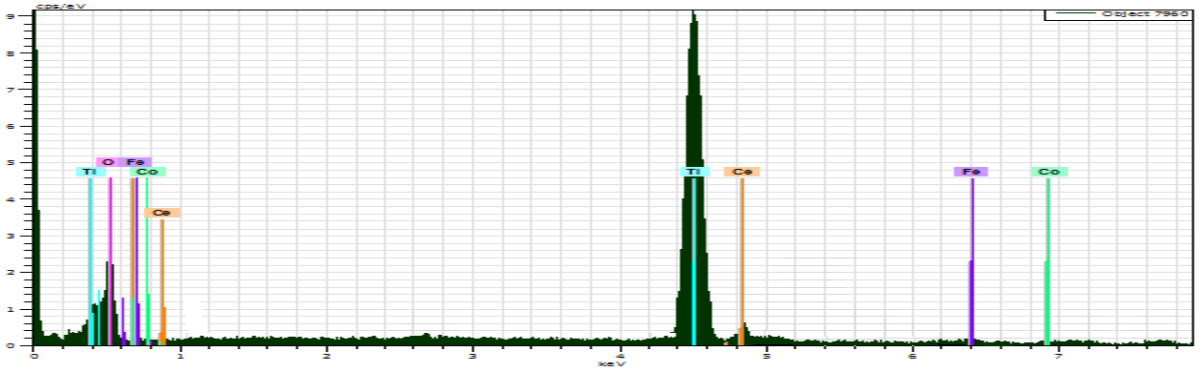

El	AN	Series	unn. C [wt.%]	norm. C [wt.%]	Atom. C [at.%]	Error [%]
Ti	22	K-series	57.12	55.27	32.19	1.8
O	8	K-series	38.72	37.47	65.31	64.2
Ce	58	L-series	3.71	3.59	0.72	0.3
Co	27	K-series	1.92	1.85	0.88	0.2
Fe	26	K-series	1.88	1.82	0.91	0.2
		Total:	103.36	100.00	100.00	

FIG 3(a). EDXS spectra of synthesized $Co_xFe_{0.02}$ $Ce_{0.02}$ $Ti_{(0.96-x)}O_2$ nanoparticles for x= 0.02 mol %.

During synthesis process the concentrations of all the dopant were dissolved thoroughly to obtain homogenous solution to avoid aggregation effect of Co, Fe or Ce (most probably occur in oxide forms).

3.3 Morphological analysis

The surface morphology of the reaction products formed as nanoparticles was estimated by FESEM images displayed by Figure 4(a-c), which shows presence of small agglomeration. On further doping agglomeration increases could be ascribed to high surface energy of nanoparticles having decrease in particle size.

3.4 TEM analysis

The nanostructural formation of prepared nanoparticles for final composition was estimated from transmission electron microscopy (TEM) displayed in Figure 5. The estimated value of particles size is in well agreement with particle size determined from XRD.

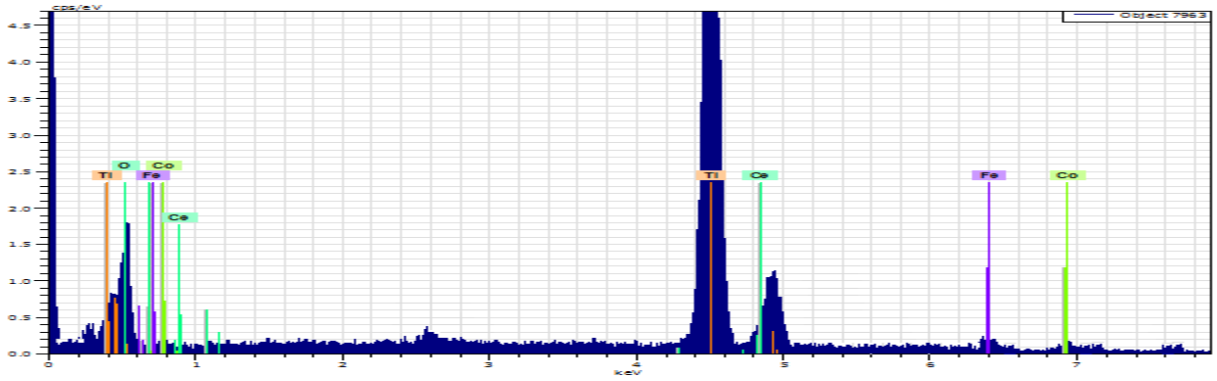

El	AN	Series	unn. C [wt.%]	norm. C [wt.%]	Atom. C [at.%]	Error [%]
Ti	22	K-series	61.78	56.73	34.55	1.8
O	8	K-series	36.98	33.95	61.89	60.6
Ce	58	L-series	4.27	3.92	0.82	0.2
Fe	26	K-series	3.03	2.78	1.45	0.2
Co	27	K-series	2.85	2.61	1.29	0.2
		Total:	108.90	100.00	100.00	

FIG 3(b). EDXS spectra of synthesized $Co_xFe_{0.02}$ $Ce_{0.02}$ $Ti_{(0.96-x)}O_2$ nanoparticles for x= 0.03 mol %.

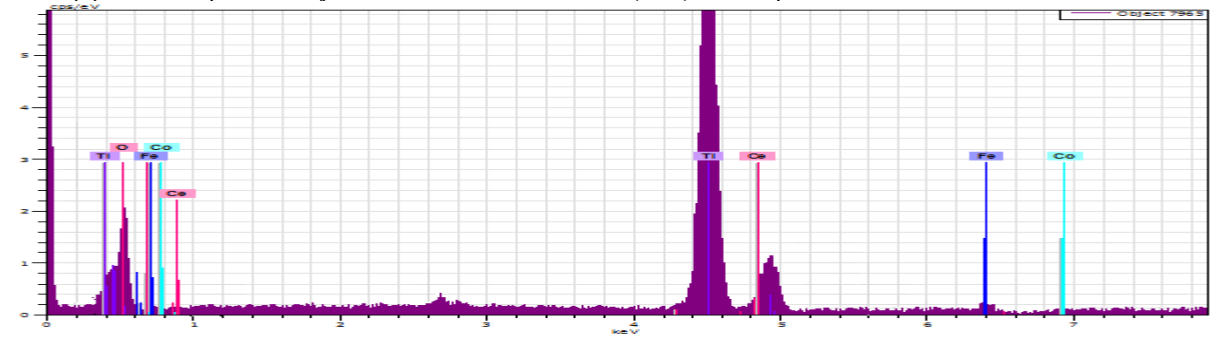

El	AN	Series	unn. C [wt.%]	norm. C [wt.%]	Atom. C [at.%]	Error [%]
Ti	22	K-series	56.72	53.89	33.92	1.7
O	8	K-series	36.53	35.88	58.87	60.2
Ce	58	L-series	4.37	4.89	1.76	0.3
Co	27	K-series	2.48	2.93	3.54	0.2
Fe	26	K-series	2.08	1.92	1.91	0.2
		Total:	102.18	100.00	100.00	

FIG 3(c). EDXS spectra of synthesized $Co_xFe_{0.02}$ $Ce_{0.02}Ti_{(0.96-x)}O_2$ nanoparticles for x= 0.04 mol %.

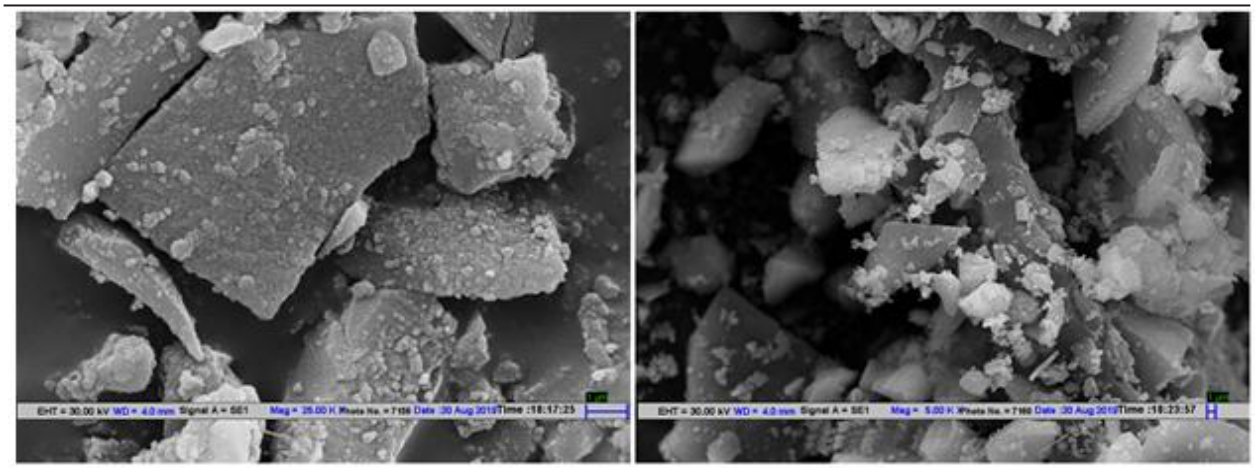

FIG 4(a-b). SEM images of synthesized $Co_xFe_{0.02}Ce_{0.02}Ti_{0.96-x}O_2$; x = 0.02 and 0.03 mol % nanoparticles.

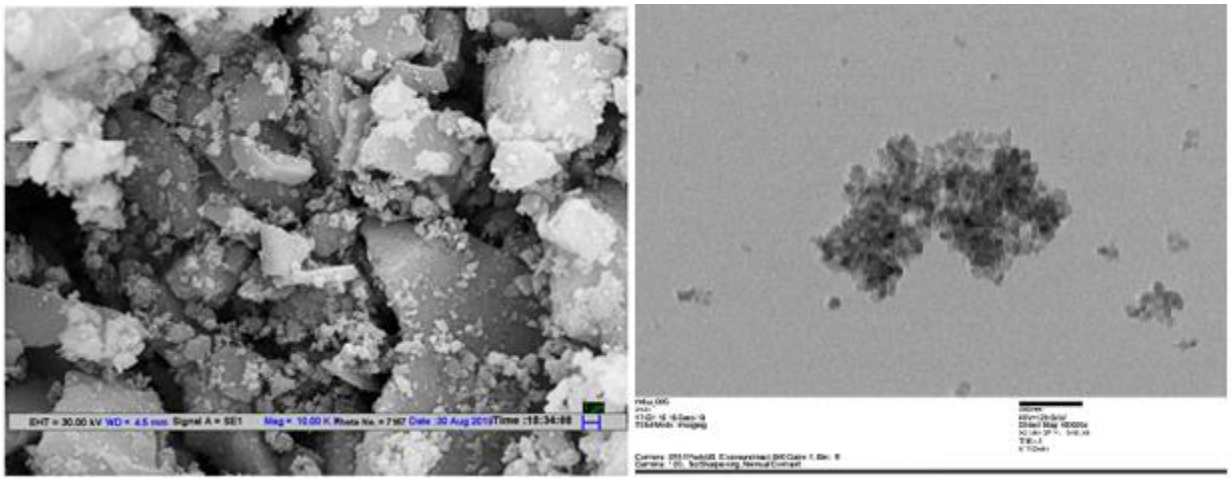

FIG 4(c). SEM image of fabricated nanoparticles for $Co_xFe_{0.02}Ce_{0.02}Ti_{0.96-x}O_2$; x = 0.04 mol %.

FIG 5. TEM image of fabricated nanoparticles for $Co_xFe_{0.02}Ce_{0.02}Ti_{0.96-x}O_2$; x = 0.04 mol %.

3.5 UV-Visible spectroscopy analysis

UV-Visible absorption spectra of co-doped TiO_2 nanoparticles is revealed by Figure 6 (a). On raising the cobalt concentration (x), absorption edge of co-doped TiO_2 nanoparticles get shifted towards region of higher wave length which corresponds to blue shift indicating formation of energy sub states within the forbidden gap. Optical band gap of formed TiO_2 nanoparticles was estimated when absorption data ($(\alpha h\nu)^{1/n}$) plotted against the energy of photon ($h\nu$) and Tauc's plot [Figure 6(b)] using following relation [15]

$$(\alpha h\nu)^{1/n} = B(h\nu - E_g) \quad (2)$$

where ν, α, E_g, n and B are frequency of radiation, absorption coefficient, band gap energy, index of semiconductor transition (n = 2 for indirect band transition), constant of proportionality respectively. Observed optical band gap values are tabulated in Table 1.

Table 1 Crystalline size and band gap values of co-doped TiO_2 nanoparticles.

Sample $Co_xFe_{0.02}Ce_{0.02}Ti_{(0.96-x)}O_2$	Angle of diffraction, 2θ (degree)	Crystalline size from XRD (nm)	Crystalline size from TEM (nm)	Band gap Eg (eV)
x=0.02 mol %	25.41	24.8	--	2.57
x=0.03 mol %	25.41	17.2	--	2.06
x=0.04 mol %	25.41	10.3	10	1.69

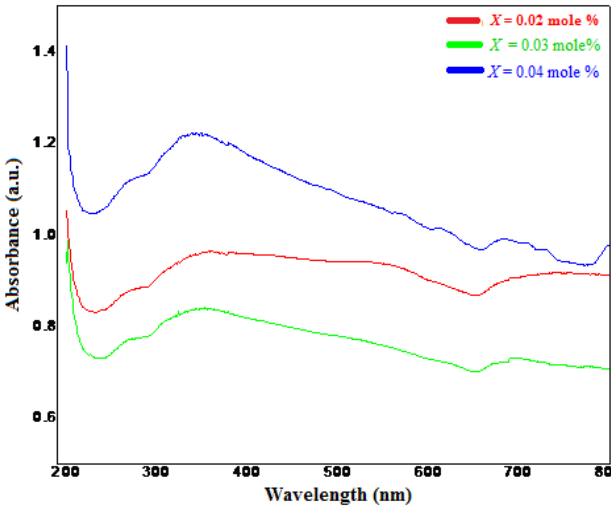

FIG 6(a). UV-Visible absorption spectra of synthesized nanoparticles.

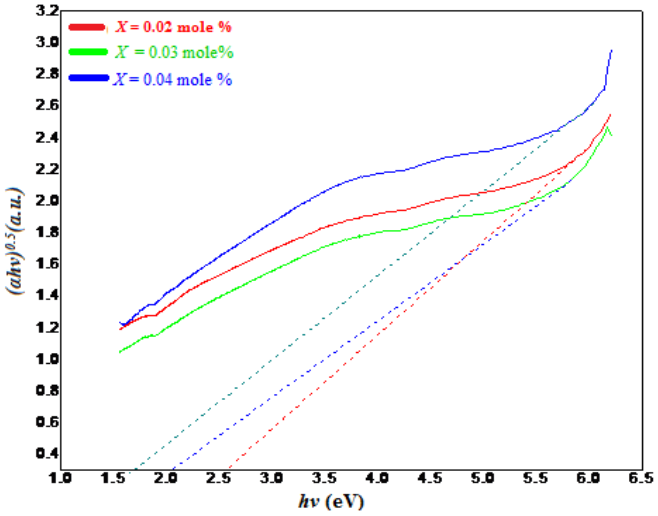

FIG 6(b). Tauc's plot of synthesized nanoparticles.

3.6 Fourier Transform Infrared analysis

The presence of structural bonds and functional groups of prepared nanoparticles was analyzed using FTIR spectra noted between 4000 cm^{-1} to 400 cm^{-1} displayed in Figure 7. Absorption band observed in spectral range 466.7 cm^{-1} to 700 cm^{-1} could attribute to (Ti-O-Ti) bending and stretching mode [16]. Absorption band observed at around 494 cm^{-1} for x = 0.02 mol % shifted to 661 cm^{-1} confirms Ti-O-Co network formation in matrix of TiO_2 [17-18]. The stable anatase phase formation is confirmed by these observations.

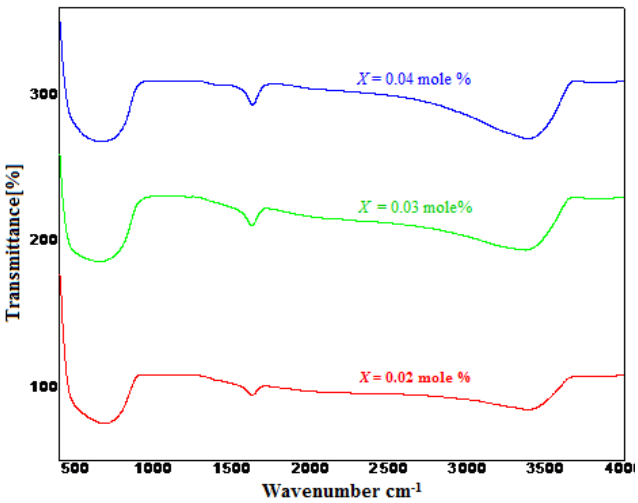

FIG 7. FTIR spectra of synthesized nanoparticles

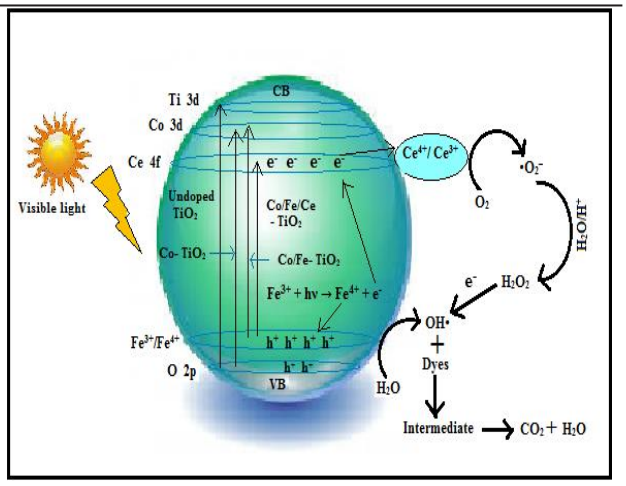

FIG 8. Charge separation mechanism of synthesized nanoparticles

Besides these vibrational bands a broad band appeared in all the samples in spectral range 4000–3200 cm^{-1} is because of (O–H) stretching vibration. Absorption peak present at 1617 cm^{-1} represents (H–O–H) bending vibrations [19].

3.5 Photocatalytic degradation activity

The principle mechanism of photocatalytic degradation is based on Langmuir-Hinshelwood kinetic model [20]. The energy level introduced by Co 3d lies below the CB (Ti 3d) and the incorporated energy level of Ce 4f further decreases the band gap as it lies below the Co 3d energy level. The position of Fe^{3+}/Fe^{4+} 3d is just above the VB (O 2p). When the surface of TiO_2 is stimulated with photons having energy equal to or higher than band gap of TiO_2, delocalization and excitation of electrons occurs from valence band to Fe^{3+}/Fe^{4+} 3d level and further from Fe^{3+}/Fe^{4+} 3d to Ce 4f produces electron-hole pairs as shown below

$$TiO_2 + h\nu \rightarrow e^-(CB) + h^+(VB)$$

The charge separation mechanism is usually based on trapping of electrons by Ce^{4+} states to reduce in Ce^{3+} state. The Ce^{4+}/Ce^{3+} serves as an electron trap centre and gives superoxide radical anions ($\bullet O_2^-$) [21-22]. These superoxide radical anions react with surface absorbed water molecules to form $HO_2^{\bullet}$ which can form hydrogen peroxide. Further reduction of hydrogen peroxide with trapped electron produces hydroxyl radical (OH•) as given below

$$Ce^{4+} + e^- \rightarrow Ce^{3+}$$
$$Ce^{3+} + O_2 \rightarrow Ce^{4+} + \bullet O_2^-$$
$$\bullet O_2^- + H_2O/H^+ \rightarrow HO_2^{\bullet}$$
$$2HO_2^{\bullet} \rightarrow H_2O_2 + O_2$$
$$H_2O_2 + e^-(\text{trapped}) \rightarrow OH\bullet + H_2O$$

The photo generated holes having high oxidation potential present in VB can oxidise adsorbed water molecule to form hydroxyl radical (OH•) as

$$h^+(VB) + H_2O \rightarrow OH\bullet + H^+$$

The hydroxyl radicals produced in oxidation and reduction can be used to degrade organic compounds present at TiO_2 surface forms intermediates H_2O/H^+. Then these intermediates produce final products by reacting with hydroxyl radicals as shown in above equations.

$$OH\bullet + \text{Organic compounds} \rightarrow \text{Intermediates} \rightarrow H_2O + CO_2$$

In case of iron, charge separation mechanism [10] is normaly based on trapping of electrons by Fe^{4+} states, to reduce Fe^{4+} in Fe^{3+} state. The Fe^{4+}/Fe^{3+} behaves as an electron trap centre and gives superoxide radical anions ($\bullet O_2^-$) as given below

$$Fe^{3+} + e^- \rightarrow Fe^{2+}$$
$$Fe^{2+} + O_2 \rightarrow Fe^{3+} + \bullet O_2^-$$
$$\bullet O_2^- + H_2O/H^+ \rightarrow HO_2^\bullet$$
$$2HO_2^\bullet \rightarrow H_2O_2 + O_2$$
$$H_2O_2 + e^- \text{ (trapped)} \rightarrow OH\bullet + H_2O$$
$$Fe^{3+} + h^+ \text{ (VB)} \rightarrow Fe^{4+}$$
$$Fe^{4+} + OH^- \rightarrow Fe^{3+} + OH\bullet$$
$$OH^\bullet + \text{Organic compounds} \rightarrow \text{Degradation product}$$

Similarly the mechanism of charge separation [23] in case of cobalt is given below

$$Co^{2+}/TiO_2 + h\nu \rightarrow Co^{2+}/TiO_2\ h^+(VB) + Co^{2+}/TiO_2\ e^-(CB)$$
$$Co^{2+} + e^- \rightarrow Co^+ \text{ (unstable)}$$
$$Co^+(\text{unstable}) + O_2 \rightarrow Co^{2+} + \bullet O_2^-$$
$$\bullet O_2^- + H_2O/H^+ \rightarrow HO_2^\bullet$$
$$2HO_2^\bullet \rightarrow H_2O_2 + O_2$$
$$H_2O_2 + e^- \text{ (trapped)} \rightarrow OH\bullet + OH^-$$
$$OH^- + h^+ \text{ (VB)} \rightarrow OH\bullet$$

The above mentioned photocatalysis mechanisms are displayed in Figure 8.

$$OH\bullet + \text{Organic dye} \rightarrow \text{intermediates} \rightarrow \text{Degradation product } (CO_2 + H_2O)$$

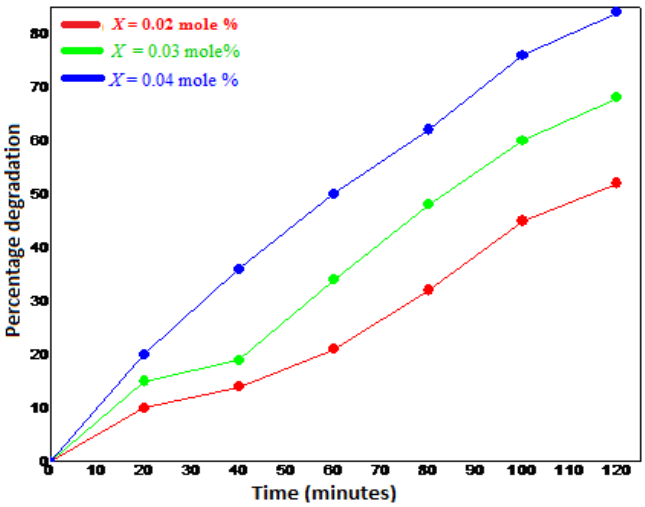

FIG. 9(a) Degradation percentage of synthesized nanopaticles against cogo red.

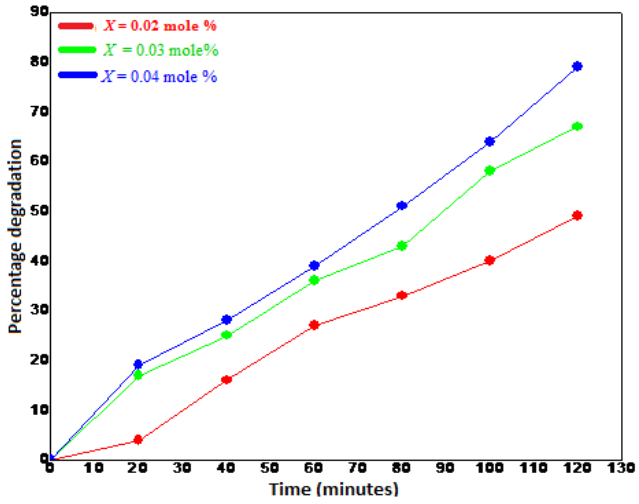

FIG. 9(b) Degradation percentage of synthesized nanopaticles against methyle orange.

The efficiency of photocatalytic degradation of prepared samples was determined using relation

$$\eta = \frac{Co - Ct}{Co} \times 100 \qquad (3)$$

Where C_o and C_t represents concentration of photocatalyst dissolved dye solution before and after illumination with visible light at time t respectively. Percentage degradation of both dyes with time are shown in Figure 9 (a & b) and the degradation efficiency are listed in Table 2. All of the doped TiO_2 nanoparticles exhibited higher photo degradation activity against both dyes, however the degradation efficiency for congo red dye is higher than methyl orange.

Table 2. Degradation efficiencies of co-doped TiO_2 ($Co_xFe_{0.02}$ $Ce_{0.02}Ti_{(0.96-x)}O_2$; x = 0.02, 0.03 & 0.04 mol %) nanoparticles.

Sample $Co_xFe_{0.02}$ $Ce_{0.02}$ $Ti_{(0.96-x)}O_2$	Percentage degradation efficiency (%) after 120 min of visible light illumination	
	Methyl Orange (MO)	Congo Red (CR)
x=0.02 mol %	49	52
x=0.03 mol %	67	68
x=0.04 mol %	79	84

4 Conclusion

Co-Fe-Ce co-doped TiO_2 nanoparticles were successfully fabricated by sol-gel technique. The formation of anatase phase and decrease in crystallite size from 24.8 nm to 10.3 nm estimated from X-ray diffraction measurements and further verified by SEM and TEM measurements. Optical band gap determined using UV–visible spectroscopy varies from 2.57 eV to 1.69 eV. The shifting of absorption edge in higher wave length region corresponds to blue shift indicate the formation of energy sub states within forbidden energy region. The presence of functional groups like (Ti-O-Ti), (Ti-O-Co), (O-H) stretching vibration and (H-O-H) bending vibration found in FTIR spectrum confirms stable anatase phase formation. Photocatalytic activitiy under visible light illumination was investigated for dyes (congo red and methyl orange) degradation. Observations shows increase of photocatalytic activity with rising concentration (x) of cobalt which is ascribed to lowering of carrier recombination rate and and increasing surface area of the fabricated nanoparticles.

REFERENCES

[1] Alex Omo Ibhadon, Paul Fitzpatrick, Catalysts 3, 189 (2013)
[2] Samira Bagheri, Nurhidayatullaili Muhd Julkapli, Rev Inorg Chem 37, 1 (2016)
[3] Pedro Magalhães, Joana Ângelo, Vera M. Sousa, Olga C. Nunes, Luísa Andrade, Adélio Mendes, Biochemical Engineering Journal 104, 20 (2015)
[4] Fujishima A & Honda K, Nature, 238, 37 (1972)
[5] Hoffmann M R, Martin ST, Choi W Y & Bahnemann D W, Chem Rev 95, 69 (1995).
[6] Yalei Zhang, Yadan Guo, Gaoke Zhang, Yuanyuan Gao, Applied Clay Science 51, 335 (2011)
[7] S. I. Nishimoto, B. Ohtani, H. Kajiwara, and T. Kagiya, Journal of the Chemical Society, Faraday Transactions 81, 61 (1985)
[8] S. H. Othman, S. Abdul Rashid, T. I. M. Ghazi, and N. Abdullah, Journal of Applied Sciences 10, 1044 (2010)
[9] Siti Hajar Othman, Suraya Abdul Rashid, Tinia Idaty Mohd Ghazi, and Norhafizah Abdullah, Journal of Nano Materials, Volume 2011 |Article ID 571601.
[10] Radha Devi Chekuri, Siva Rao Tirukkovalluri, South African Journal of Chemical Engineering 24, 183 (2017)
[11] Fatemeh Mostaghnia, Yasaman Abed, Materials Research 19 741 (2016)
[12] Ibram Ganesh, Polkampally P. Kumar, Abhishek K. Gupta, Panakati S.C. Sekhar, Kalathur Radha, Gadhe Padmanabham, Govindan Sundararajan, Processing and Application of Ceramics 6, 21 (2012)
[13] Xiao-jun Lia, De-jun Sib, Jun Fangb, Zhi-quan Jiangb, Wei-xin Huang, Chinese Journal of Chemical Physics 19, 539 (2006)
[14] B.D. Cullity, Elements of X-ray Diffraction, Reading Mass: Addison–Wesley Publishing Co. (1956) 352.
[15] D.A. Davis, Japanese J Appl. Phys, 32 178 (1993).
[16] R.Sharmila Devi, R.Venckatesh, Rajeshwari Sivaraj, International Journal of Innovative Research in Science 3,

15206 (2014)
[17] A Nixon Thangaraj, C Ravi Samuel Raj, W Jose Benita Regilet, Journal of Chemical and Pharmaceutical Research 9, 257 (2017)
[18] T. Sivarao, D. C. Radha **,** Nanoscience & Nanotechnology 11, 1 (2017)
[19] M. Manzoor, A. Rafiq, M. Ikram, M. Nafees, S. Ali, International Nano Letters 8,1 (2018)
[20] Pedro Magalhães, Luísa Andrade, Olga C. Nunes, Adélio Mendes, Review Advanced Material Science 51, 91 (2017)
[21] Venkat Savunthari Kirankumar, Shanmugam Sumathi, Environmental Science and Pollution Research, 26 19189 (2019)
[22] Bruno A. T. Menezes, Daniel E. B. Moreira, Hugo A. Oliveira, Lippy F. Marques, Juliana F. Lima, J. Braz. Chem. Society 3, 153 (2020)
[23] Zoltan Ambrus, Nandor Balazs, Tunde Alapi, Gyula Wittmann, Pal Sipos, Andras Dombi and Karoly Mogyorosi, Applied Catalysis B: Environmental 81, 27 (2008)